PROCEEDINGS, 41st Workshop on Geothermal Reservoir Engineering
Stanford University, Stanford, California, February 22-24, 2016
SGP-TR-209

Play Fairway Analysis for Structurally Controlled Geothermal Systems in the Eastern Great Basin Extensional Regime, Utah

Philip E. Wannamaker[1], Kristine L. Pankow[2], Joseph N. Moore[1], Gregory D. Nash[1], Virginie Maris[1], Stuart F. Simmons[1] and Christian L. Hardwick[3]

[1]University of Utah/Energy & Geoscience Institute, 423 Wakara Way, Ste 300, Salt Lake City, UT 84108 USA
[2]University of Utah/Dept of Geology & Geophysics, 115 S 1460 E, Rm 211 FASB, Salt Lake City, UT 84112 USA
[3]Utah Geological Survey, 1594 W. North Temple, Ste 3110, Salt Lake City, UT 84114 USA

pewanna@egi.utah.edu

Keywords: play fairway analysis, eastern Great Basin, exploration, GIS

ABSTRACT

A research team with membership from the University of Utah/Energy & Geoscience Institute, and the University of Utah/Dept. of Geology & Geophysics, have carried out a play fairway analysis (PFA) for geothermal resources in the Eastern Great Basin extensional tectonic regime of western Utah. Here, active Basin and Range (B&R) extension with volcanism having a N-S strike is superimposed upon pre-existing E-W belts of plutonic rocks and large-scale structural lineaments. Cumulative heat flow along the N-S strike of the state totals approximately 5 GW above background stable interior. Three electricity producing power plants currently exist with potential for greatly increasing this number. Our PFA adds to understanding of the potential sources of heat and permeability in the region, which are the two principal criteria for establishing a geothermal resource. An advantage of this PFA region is the relative abundance of existing data, related to a substantial history of geothermal exploration in the region.

Criteria selected for establishing heat potential include direct heat flow measurements in boreholes, magnetotelluric (MT) low resistivity anomalies, fluid geochemistry, and proximity to recent volcanic eruptions. Permeability is established by fault density, by identification of critically stress areas, and MT low resistivity anomalies. Heat source and permeability potential are expressed in terms of their individual common risk segment maps, with a color scheme using green for most favorable (low risk) and red for least favorable (high risk). Due to data quantity, statistical approaches to defining risk, together with good conceptual models of the area, lead to several followup recommendations. Two east-west conductive lineaments, one coincident with the Cove Fort transverse zone and one nearby to the north which we name the Twin Peaks-Meadow zone, appear to be controlling structures for several local fluid and heat upwellings such as Cove Fort, Twin Peaks, and several previously unnamed prospects. Priorities for followup include southward swath extension and detailed fill-in MT coverage, passive helium transect surveying, and detailed structural investigation.

1. INTRODUCTION

Play Fairway Analysis (PFA) in the geothermal context combines regional geological/ geophysical understanding with knowledge of prospect control elements (e.g., origin of heat, pathways to heat up and concentrate fluids)to produce an inventory of prospect leads (see Fraser, 2010, for an oil and gas analog). The potential for new discoveries should be increased dramatically in regions where active magmatism creating a large heat endowment occurs in conjunction with diverse structural trends some of which may be well oriented to create reservoir space. Thus we have been drawn to examine the active eastern Great Basin of western Utah. Here, active N-S striking extension with high-temperature, bimodal volcanism (Bendersky et al., 2012) cross-cuts E-W trending plutonic belts of mid-Cenozoic age including including large transverse structures of this age or greater (Wannamaker et al., 2008) (Figure 1).

Our approach to reassessing geothermal resource potential in this region emphasizes application of MT geophysics, fluid geochemistry and structural geology to resolve heat source and permeability. The approach incorporates heat flow, volcanic distributions, multi-component geochemistry, and geothermal system modeling from a global context. It draws upon our experience elsewhere in the extensional Great Basin where producing geothermal systems are characterized by crustal-scale, low electrical resistivity roots resolved from MT surveying that connect to deep magmatic activity (Wannamaker et al., 2007, 2011; Siler et al., 2014). Such systems lie also in favorably dilatent structural settings and appear to have isotopic compositions (He, O, C) indicative of deep high-T input. In this PFA project, we seek to identify areas in the eastern Great Basin containing systems with such characteristics as priority areas for followup.

2. BACKGROUND AND ASSUMPTIONS

In extensional (rift) systems, exhumation of the crust elevates the geotherm and creates fracture permeability (e.g., Henley and Ellis, 1983). Induced circulating fluids tend to be neutral pH and Cl bearing with modest salinity (1-2 wt %). A common model for geothermal systems here involves deep circulation of waters driven by topographic flow to depths potentially of 10 km near the brittle-ductile lithologic transition (Wisian and Blackwell, 2004). Other high temperature extensional systems clearly have magmatic affinities given nearby volcanism and other evidence such as He isotopes (e.g., Simmons et al., 2015).

GPS-based geodesy shows that present-day extension rates at the surface are ~4 mm/yr cumulative from the Wasatch Front to the Nevada border (Kreemer, 2012). Western Utah contains the most pronounced seismic tomography anomalies in its upper-most mantle of the entire U.S. apart possibly from the eastern Snake River Plain (Schmandt and Lin, 2014) signifying strong degrees of melting. A pronounced N-S trend of Quaternary basaltic and bimodal magmatism runs the length of the state of Utah, extending into the Grand Canyon of Arizona and to the Snake River Plain of Idaho (Nelson and Tingey, 1997) (Figure 1). The basaltic magmatism feeding into the crust is interpreted to be the hottest of the Great Basin (Bendersky et al., 2012). The thermal processes of extension under the eastern Great Basin are responsible for cumulative heat flow along the N-S strike of the state totalling approximately 5 GW above background stable interior (map in Edwards and Chapman, 2013).

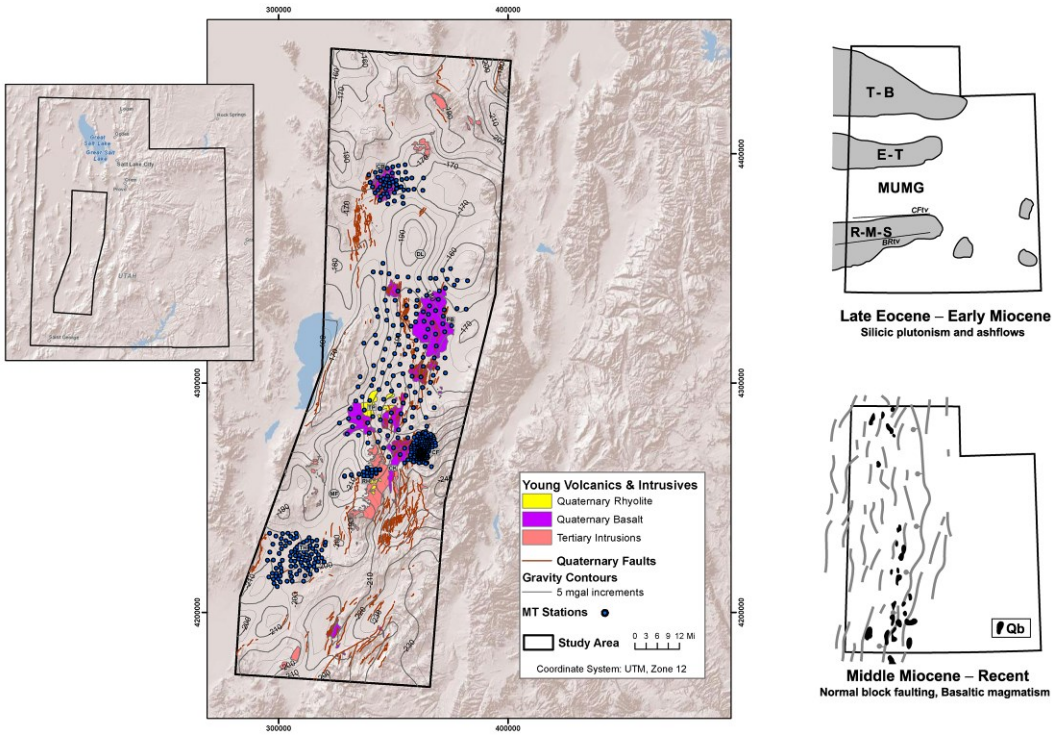

Figure 1: Left: DEM map of western Utah showing extension-dominated physiography. Black polygon represents play fairway of our project with 5 mgal gravity contours. Producing geothermal systems include Roosevelt Hot Springs (RHS), Cove Fort (CF) and Thermo (TH). Important Q volcanic extrusives are Crater Bench (CB), Pavant Butte (PB), Twin Peaks (TP) and Crater Knoll-Red Knoll (CK). Urban centers are Delta (DL) and Milford (MF). Upper right: Middle Cenozoic tectonism in Utah is dominated by voluminous plutonism in E-W belts: Tuscarora-Bingham (T-B), Eureka-Tintic (E-T) and Reno-Pioche-Marysvale-San Juan (R-M-S) separated by mid-Utah magmatic gap (MUMG). Lower right: Mid-Miocene to present Basin and Range extension overprints previous tectonic and plutonic episodes creating numerous intersecting trends and magmatic heat sources. Quaternary basalts (Qb) of abnormally high potential temperatures are erupted in a N-S trend the length of the state.

We are modernizing understanding of geothermal prospectivity of the eastern Great Basin by emphasizing a combination of magnetotellurics (MT), structural geology, and fluid chemistry integrated in a context of heat flow and volcanology. High-temperature geothermal systems elsewhere in the Great Basin including Dixie Valley and McGinness Hills show MT low-resistivity roots connecting to probable magmatic underplating and fluid release in the deep crust (Wannamaker et al., 2007, 2011, 2013a,b) (Figure 2). Such roots represent large-scale permeability and potential heat upwelling. Thus we examine available MT data in the extensional eastern Great Basin in a fully 3D fashion for such roots as evidence toward the existence of previously blind geothermal systems.

The Great Basin studies above also showed that high-temperature systems lie in structural geological settings favorable for dilatency. The generally N-S striking rift faults are obvious on geological maps. However, our PFA area is noteworthy for the existence of fundamental E-W structural lineaments associated with emplacement of major belts of plutonic rocks in the middle Cenozoic prior to rifting (Neilson et al., 1986; Rowley et al., 1998a,b, 2001). Four major lineaments are recognized in our PFA area (Figure 3), three directly from structural geology and one that will emerge from MT data modeling. Intersection of faults of diverse trends under a deformational regime is a prescription for dilatency and the creation of space and permeability for geothermal fluids (e.g. Faulds et al., 2013). The Dixie Valley and McGinness Hills systems also exhibited elevated ^{3}He content in sampled fluids confirming mantle magmatic geochemical contributions suggested by the MT resistivity structure. Thus the three methods of MT, structural geology, and fluid geochemistry will be combined in our study to infer the likeliest zones of high-temperature upwelling into favorable structural situations.

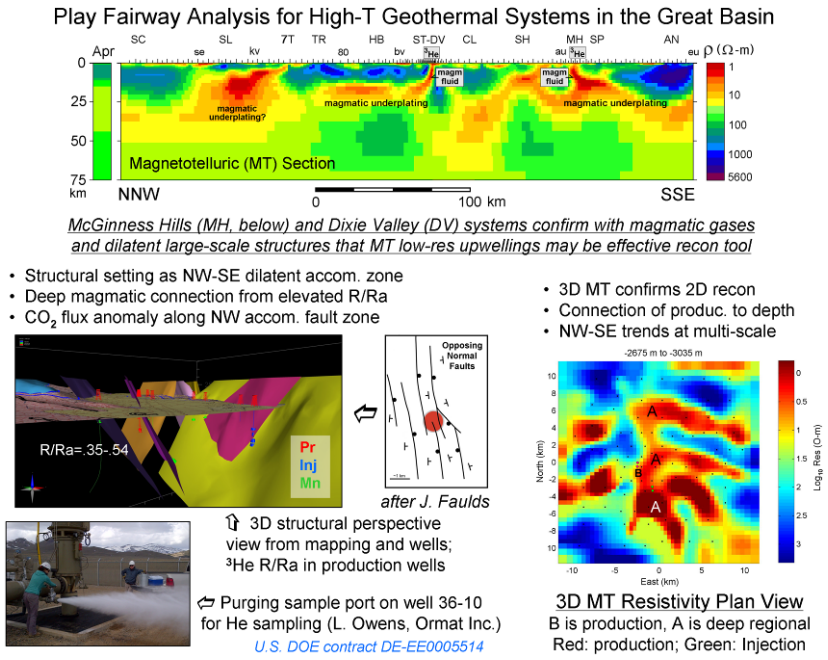

Figure 2: Illustration of integrative interpretation of the McGinness Hills NV moderate temperature geothermal system. Regional MT transect studies (top) uncovered several low-resistivity bodies in the deep crust ascribed to magmatic underplating and hydrothermal fluid release. Such systems in turn lie in 3D structural zones promoting dilatency. Sampled fluids show isotopic compositions confirming magmatic input. Study by Wannamaker et al. (2013b).

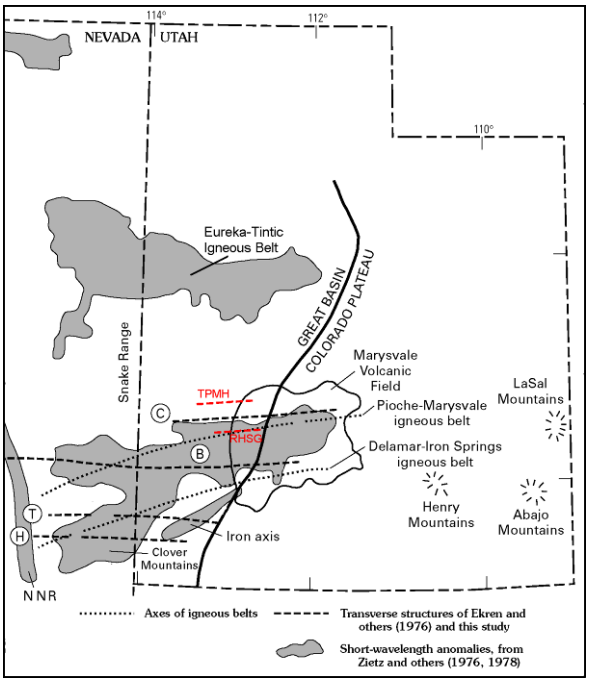

Figure 3: Major igneous and tectonic features of southern and central Utah and southeastern Nevada, modified from Rowley (1998a). Added are interpreted lineaments of Twin Peaks-Meadow Hatton (TPM) and Roosevelt Hot Springs graben (RHG). Other lineaments include Cove Fort (C), Blue Ribbon (B), Timpahute (T) and Helene (H). NNR is Northern Nevada Rift. Not shown also are E-W Payson and Sand Pass lineaments in the Eureka-Tintic igneous belt plus the Tuscarora igneous belt and its lineaments of northern Utah (Rowley et al., 1998a).

The relative abundance of data in our PFA area will allow useful common risk segment (CRS) maps of heat source and permeability to be derived. Ideally, risk distributions would be computed from a family of spatially continuous inputs represented in the depicted flow diagram. Most of the inputs at hand are sufficiently sampled to derive a probability function which, together with meta-rankings of inputs, provide quantitative CRS distributions.

3. WORKFLOW AND RESULTS

At the outset, pertinent data to do PFA were assembled for the eastern Great Basin region. These include: 1), a large number of MT site response functions; 2), earthquakes from the Utah Seismic Network for clustering analysis; 3), fault locations and orientations from the USGS and Utah Geological Survey (UGS) active fault databases and the literature; 4), major element and isotopic compositions of spring fluids from the USGS and UGS databases and published/unpublished literature; 5), heat flow from the SMU database greatly augmented by temperature gradient holes culled from industry records; and 6), volcanic distributions from the Utah Geological Survey database. Subsequently, data were processed using state-of-the-art modeling approaches (some very new) to obtain modern 3D geophysical images, an updated active fault database, identification of critically stressed zones from potential fields and aerial photography, a re-evaluation of chemical geothermometry, conceptual models of geothermal resources in this region, and common risk segment maps for heat, permeability and prospectivity in the eastern Great Basin.

3.1 Magnetotelluric Resistivity Structure

Available MT data for the project include 470 soundings acquired by contract for the State of Utah, Enel Inc, and Cyrc Inc. These are a mix of dense clusters at individual thermal areas (Crater Bench, Cove Fort, Thermo) and a wide swath at somewhat greater average spacing over the broader Sevier Basin and northern Mineral Mountains (Figure 1) (Wannamaker et al., 2013c; Hardwick et al., 2015). The 3D resistivity images are produced using a new edge finite element algorithm also developed under DOE/GTP support described in detail by Kordy et al (2016a,b). This algorithm simulates topography precisely using deformable hexahedral elements and uses the entire MT tensor set of 12 quantities (four complex impedance elements and two complex tipper elements) per frequency per site. The solution of all system matrices is direct (non iterative), making use of the Intel MKL matrix packages PARDISO for the sparse finite element system and PLASMA for the full parameter step matrix. The latter matrix is formulated in data space for compactness.

We performed 3D MT inversions of the clustered site sets over the Crater Bench, Cove Fort, and Thermo geothermal systems as well as the broad swath coverage over the Sevier Basin and northern Mineral Mtns. The Sevier Desert data set covers an elongate swath from Delta city southward through the desert and onto the northern Mineral Mountains where basement rock may be dominated by mid-Cenozoic granodiorites of the RMS trend (Figure 1). The central portion of the finite element mesh is given in Figure 4. There are 143 stations over the prospect and the period range used is 0.08 through 212 s. Cell widths among the sites typically are 800 m wide and the total finite element mesh is 140 (N) x 101 (E) x 62 (Z) cells with the upper 12 element layers devoted to the air. A narrow rim of finite elements around the mesh sides and bottom is kept fixed so the inversion domain is 137 x 98 x 46 = 617,596 parameters. Error floors were 3.5% of max{ |Zij| ; |Zxy-Zyx|/2 } and 0.03 tipper for tipper. The starting model was 25 ohm-m and a final nRMS of 1.7 was achieved monotonically in 12 iterations. Run times were 13.5 hours/iteration.

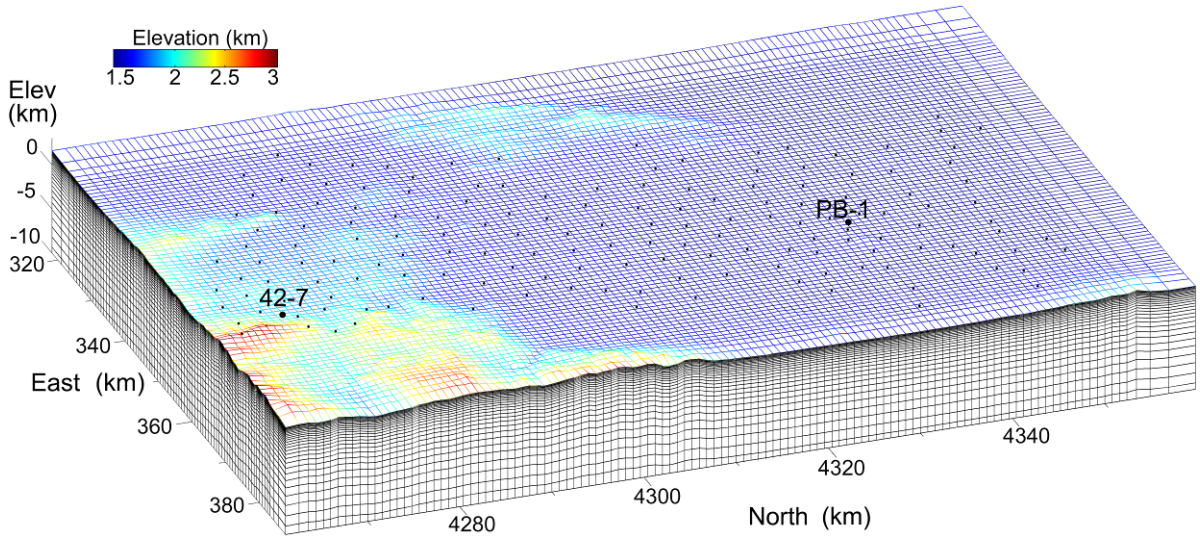

Figure 4: Central section of finite element model inversion mesh for the Sevier Desert MT data set. Topography is represented through gradual distortion of the hexahedral elements and color coded for elevation. Wells from Cove Fort (42-7) and Pavant Butte (PB-1) thermal areas noted.

At relatively shallow levels (1.4 km), the model is dominated by low resistivity of the late Tertiary sediments of the Sevier Basin and, in the southwestmost corner of the model, the Milford Valley sediments (Figure 5). At deeper upper crustal levels (4.5 km) below the Cenozoic sedimentary section, a conductive albeit fainter N-S axis remains below the trend of Quaternary basalts through the Sevier Desert. The Pavant Butte 1 well is located at the eastern margin of this axis. Within MT station sampling and inversion smoothing, we do not believe there is a fundamental conflict with well log readings showing resistive rocks at ~3 km depth (Hardwick et al., 2015). Additional MT sounding data could improve inversion resolution here. This large conductive axis largely terminates to the south at the latitude of Twin Peaks Quaternary bimodal volcanic center (northing 4295 km), at and beyond which any conductive structures are more clumped and non-lineated at this depth. Such localized conductors appear associated with Twin Peaks and with Cove Fort. There also is a third conductor not associated with a previously investigated geothermal occurrence north along strike from the Quaternary Crater Knoll-Red Knoll basaltic intrusive (CK). In this general area, the conductors reside in what should be predominantly mid-Tertiary granodioritic basement of the RMS belt.

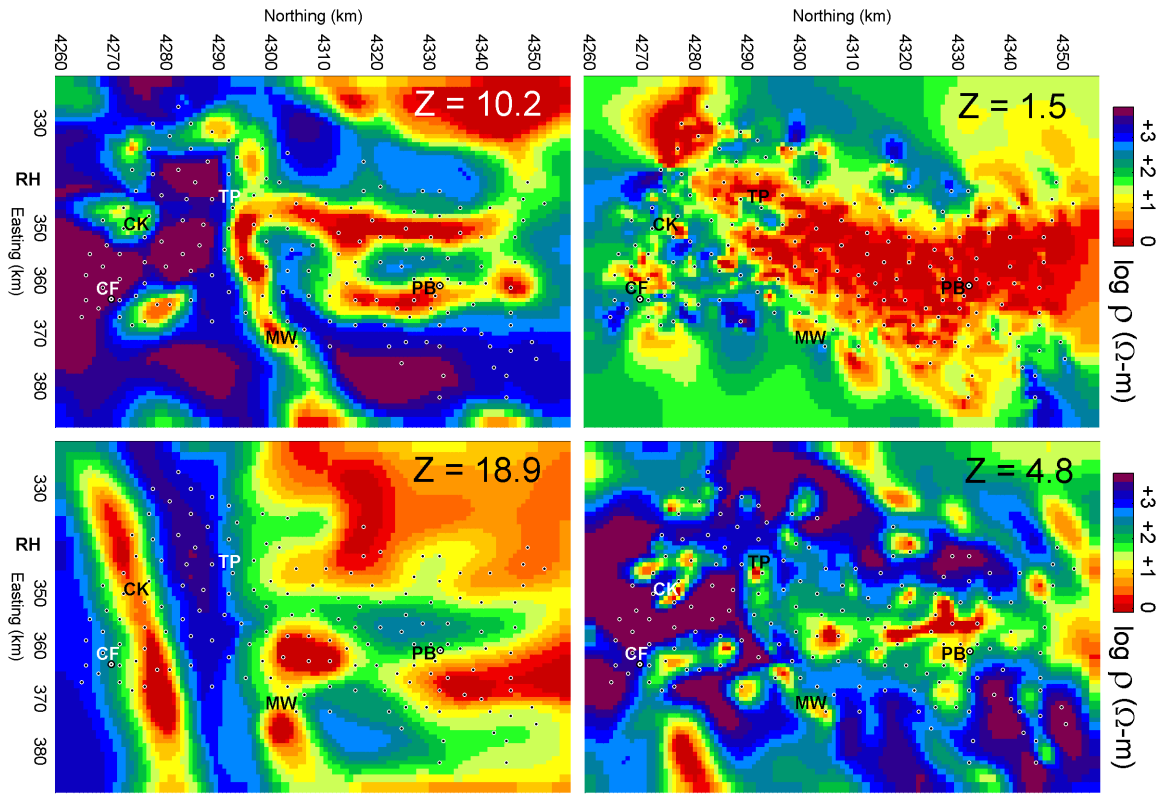

Figure 5: Central section of finite element model inversion mesh for the Sevier Desert MT data set. Topography is represented through gradual distortion of the hexahedral elements and color coded for elevation. Wells from Cove Fort (42-7) and Pavant Butte (PB-1) thermal areas noted.

Deeper in the model (10.2 km) of Figure 5, the Cove Fort and Crater Knoll-Red Knoll conductors persist although that of Twin Peaks has merged with a pronounced E-W linear conductor bounding highly resistive basement rocks of the R-M-S belt immediately to the south. At its east end, this linear conductor underlies the Meadow-Hatton thermal springs. We identify this as one of the four principal E-W lineaments in the project area and include it in collection in Figure 3. Under a regime of E-W extension, these auxiliary structures may suffer dilatency and provide conduits for upward geothermal fluid flow. Below the Sevier Basin to the north, the central linear basement conductor has bifurcated into two parallel N-S conductors that have divergent dips west and east. This split was observed also in the inversion model of Wannamaker et al (2013c) using a different algorithm. The abrupt, E-W oriented northern boundary of the R-M-S plutonic belt appears to continue to the east and separate the Cove Fort area from the Sevier Basin. At the deepest levels shown (18.9 km), a second E-W linear conductor of high amplitude unites the Crater Knoll-Red Knoll and Cove Fort conductors. In fact, it appears to continue eastward and project toward the Joseph and Monroe geothermal occurrences in Sevier Valley. This structure appears to bear a close relationship to the Cove Fort transverse zone (Figures 1 and 3), comprised of large-scale faulting, downwarps and igneous centers (Rowley et al., 1998; Rowley and Dixon, 2001). Further MT data coverage is needed to the south to determine if fundamental low resistivity structures may be associated with the Roosevelt Hot Springs or reveal further controlling lineaments and exhibit a relationship to those shown by the current data. Such may be expected given the pronounced E-W graben structure entering the Roosevelt geothermal system from the east (Nielson et al., 1986).

3.2 Seismic Swarm Analysis

Clustering of earthquakes located in the PFA study box was redone using Cluster2000 (Reasenberg, 1985) software for the years 1981-2014. We were able to recover the clusters previously identified by Arabasz et al. (2007), plus additional clusters. Interestingly, swarm clusters and non-swarm clusters occur in the same areas (Figure 6). Unfortunately, the Utah Seismic Network lies mainly to the east and is sparse in the geothermal areas, so double-difference relocation showed little improvement. Despite these limitations, swarms are identified with the Cove Fort and Roosevelt Hot Springs geothermal systems, and with the newly found MT conductor named the Cinder Knoll (CK) conductor, suggesting that seismic swarms are fluid-related.

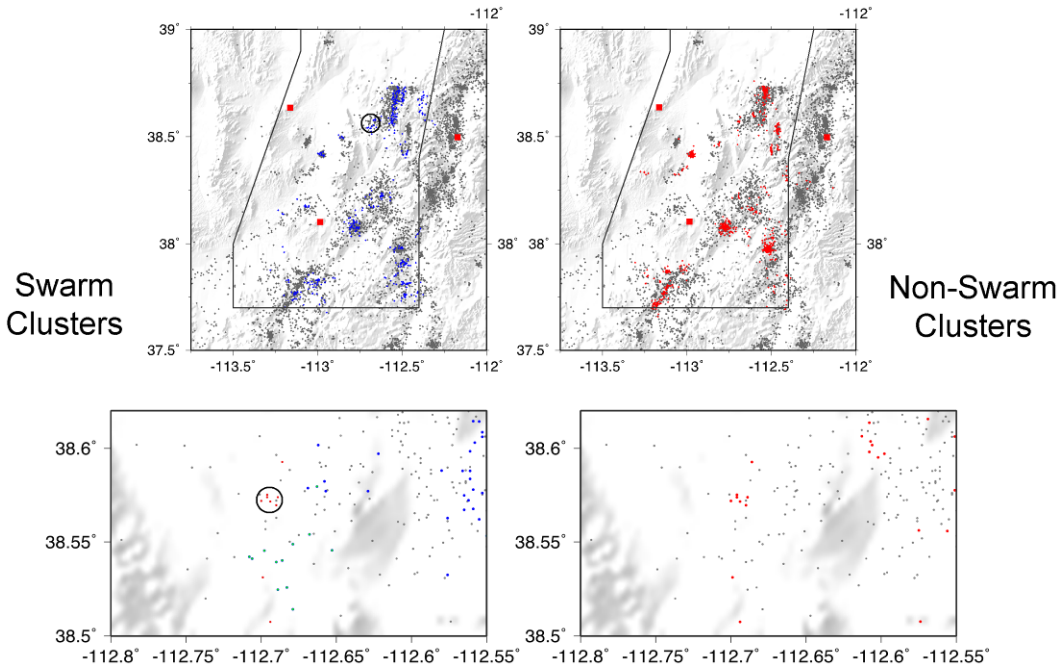

Figure 6: Location of events that form swarm (left) and non-swarm (right) clusters. Top: Southern half of PFA study area. Gray dots are events in the UUSS catalog; Blue dots, events that form swarm clusters; Red dots, events that form non-swarm clusters. Red squares are seismic stations. Bottom: Focus on area near Crater Knoll (CK). Left, swarm clusters (red, green and blue). Green stars show events first identified in the Arabasz et al. (2007) for a swarm that occurred in 1987; Red stars a second swarm in the same general location identified in this analysis; Blue dots, events forming additional clusters. A black circle is drawn around the cluster associated with the CK conductor. Right, events forming mainshock-aftershock clusters (red).

Recent improvements to cluster detection through treatment of recording gaps and waveform timing are now yielding much smaller events. Focusing on the newly found conductor in the Crater Knolls area on the northeast side of the Mineral Mtns, data from 2005 were clustered based on waveform similarity allowing construction of subspace detectors (Harris, 2006; Harris and Paik, 2006; Chambers et al., in press) to identify other earthquakes. Using this subspace method, we were able to find 30 additional events down to near M0 (Figure 7). This is a promising advance and will be pursued in the Phase II field campaign using our new Nodal 3C instrument pool.

3.3 Structural Geology

We have combed the USGS and UGS Quaternary data bases for areas of high fault density and for favorable settings for dilatency such as relay ramps, horse-tailing terminations, step-overs, fault tips, accommodation zones, and fault intersections. . We have identified 35 areas with promising structural geometries for fracture permeability within the play fairway and nearby areas, interpreted from geomorphology and gravity data. Criteria included (1) the structural setting must be related to Quaternary seismicity (mapped as Quaternary fault(s) or spatially related to historical earthquakes), and (2) the geometry must be known to produce long-term critical stress as defined by the prior favorable setting types.

An example structural zone is shown in Figure 8. This sub-region is dominated by a NNW striking-NE dipping, Quaternary normal fault system with intersections, fault tips, and an accommodation zone bounding its southern extent. Quaternary basalt flows are also found in this area and the Cove Fort lineament projects into it. The intersection of this NNW fault and the ENE Cove Fort lineament corresponds to the strong MT low-resistivity upwelling presented in Figure 5. We have found that a significant number of stressed areas are either directly related or in close proximity to MT conductors.

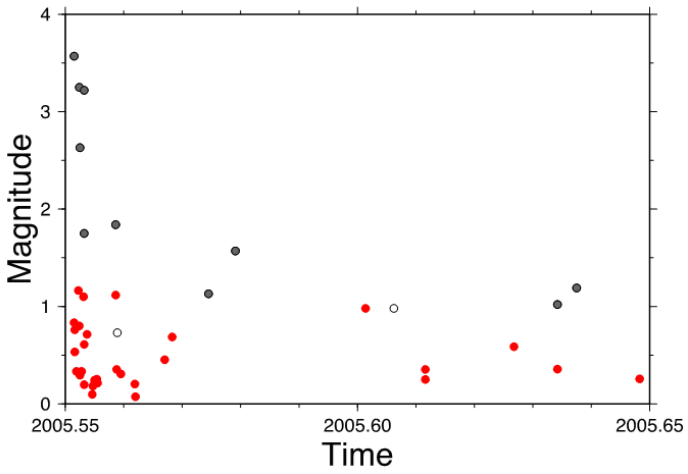

Figure 7: Time magnitude history for the 2005 sequence that occurred near the new MT structure east of the Mineral Mountains. Grey circles, events used to build the subspace. Red circles, newly detected earthquakes.

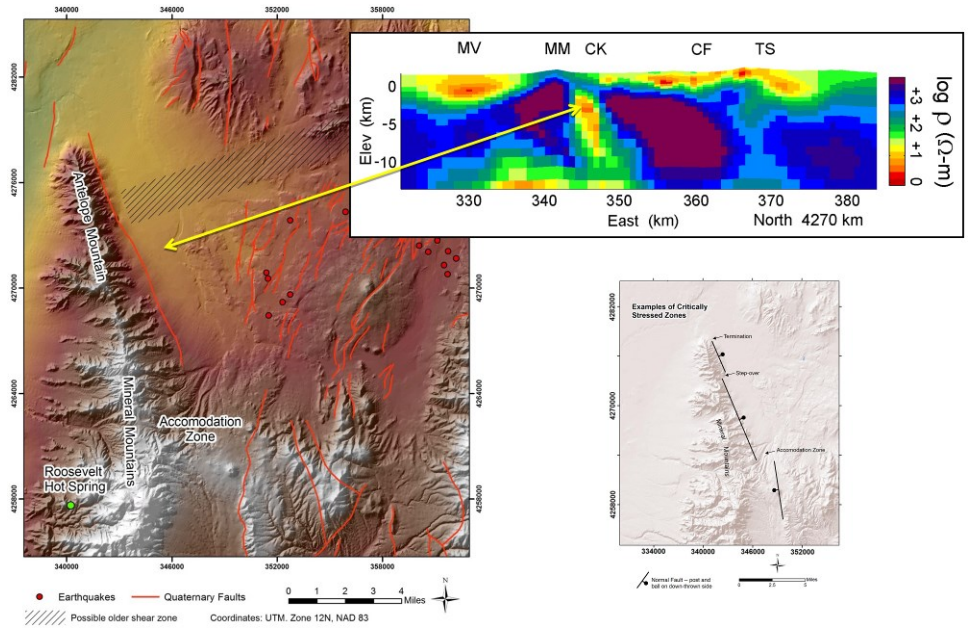

Figure 8: Left: DEM plot of northern Mineral Range showing Quaternary faults in red and the suspected transverse zone is as hatchured band. Northern end of Cunningham Wash is visible below label Accommodation Zone. Upper right: section view through 3D MT resistivity inversion model at a northing near the intersection of major Quaternary fault and older transverse zone showing the Cinder Knoll conductor. Physiographic features include Milford Valley (MV), Mineral Mountains (MM), Crater Knoll-Red Knoll (CK), Cove Fort (CF), and Tushar Mountains (TS). Lower right: Detailed view of critically stressed zone on northeast side of Mineral Mtns exemplifying features of choice.

3.4 Geochemistry and System Modeling

Most of the 100+ compiled thermal water samples from the UGS data base can be classified as chloride, sulfate or hybrid chloride-sulfate waters (Figure 19). Cove Fort and Roosevelt Hot Springs (RHS) waters have similar chloride-sulfate concentrations, despite different reservoir rocks (carbonates versus siliceous gneiss/granite). Elevated 3He/4He isotope ratios at RHS (2.25 R/Ra), Cove Fort (0.62) and Thermo (0.9 R/Ra) imply a mantle-sourced magmatic component, confirming our original exploration paradigm depicted in Figure 2. The positive correlation between aqueous silica, reservoir temperature, and the quartz solubility curve for production waters (Cove Fort, Roosevelt, Thermo) indicates that quartz-silica geothermometry may give the most reliable minimum resource temperatures when applied to spring waters (Figure 9). Na/K geothermometry is consistent with measured temperatures at RHS, but high apparent

Na/K values for Cove Fort and Thermo suggest yet higher temperatures below the producing reservoir (Simmons et al., 2015). This characteristic, plus others such as water chemistry not solely compatible with the immediate reservoir rocks of production, indicates that fluid circulation volumes in the eastern Great Basin systems are large suggesting similar producing potential.

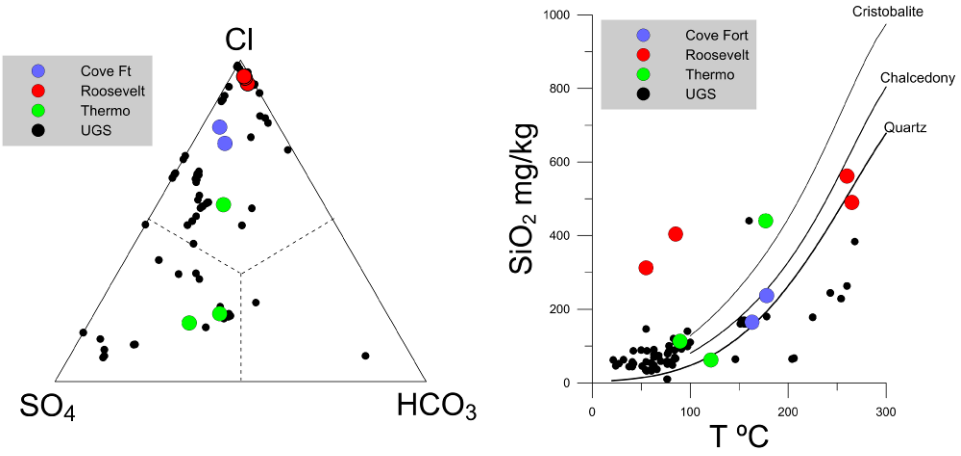

Figure 9: Left (a): Cl-HCO3-SO4 ternary diagram showing the compositions of thermal waters in southwestern Utah using data from the UGS data base (Cole, 1983; Blackett and Wakefield, 2002), Cove Fort (Moore et al., 2000), Roosevelt (Capuano and Cole, 1982), and Thermo (Moore, unpublished). Right (b): Comparison of aqueous silica concentrations and temperatures for thermal waters, the highest silica values correspond to production waters from Roosevelt. Solubilities of quartz, chalcedony and cristobalite (Fournier, 1991) are shown for comparison.

A heuristic composite model for geothermal systems in the eastern Great Basin is offered in Figure 10. Thermal waters at Cove Fort, Roosevelt, and Thermo involve deep circulation of meteoric waters subsequently modified by hot water-rock interaction (>250 C) (Blackett, 2007; Simmons et al., 2015). Geological evidence suggests that the main deep lithology is made up of crystalline basement rocks (i.e., gneiss, granite). The precise source of aqueous Cl, SO4, and HCO3 are unclear, but the occurrence of young volcanic centers along with anomalous helium isotope ratios open the possibility that some portion comes from intruding magmas similar to geothermal fluids in volcanic regions (e.g., Giggenbach, 1997). Thermal spring water compositions suggest they are fed by separate isolated geothermal systems, then modified by interaction with salts and clays either in alluvial basin fill or in subjacent Mz-Pz sedimentary rocks. In sediment-dominated cases, Na/K geothermometry is unlikely to be reliable. Presence of 3He suggests that the regional Sevier thermal anomaly owes its origin to deep intrusion of magma(s). The large regional endowment of thermal energy associated with hot basement rocks suggests there is considerable potential for finding blind resources including those occurring in deep sedimentary aquifers and EGS reservoirs (Allis et al., 2015a,b).

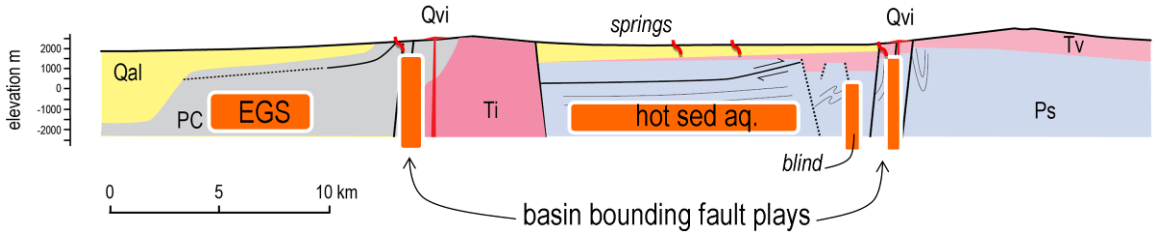

Figure 9: Highly simplified, 2-D cartoon representing geothermal systems in the eastern Great Basin. Systems tend to be discrete and isolated. Depiction allows for possibility that substantial sections of sedimentary rock such as under Sevier Basin may be heated by deep magmatic activity.

4. COMMON RISK SEGMENT (CRS) MAPPING

Following the cataloguing of pertinent available data sets in the eastern Great Basin, discussion of their individual implications for hydrothermal conditions in the subsurface, and a possible occurrence model for resources in the PFA area, we turn now to quantifying prospective subareas to the extent that probabilistic and multi-criteria decision making (MCDM) approaches allow (Figure 11). One crucial technical aspect is accommodating diverse types of data with varying units and ranges. We approach this through the probability kriging technique in the ArcGIS statistical toolbox. For different data types, we ask what is the probability on a scale of 0 to 1 that the particular data type will exceed a certain threshold considered favorable for a resource, or at least favorable for followup investigation. Some of the data are too sparse to allow this, such as some of the geochemical spring sampling. Data such as these are used to support or downplay resource likelihood in different areas. Following is a discussion of appropriate probability kriged data sets.

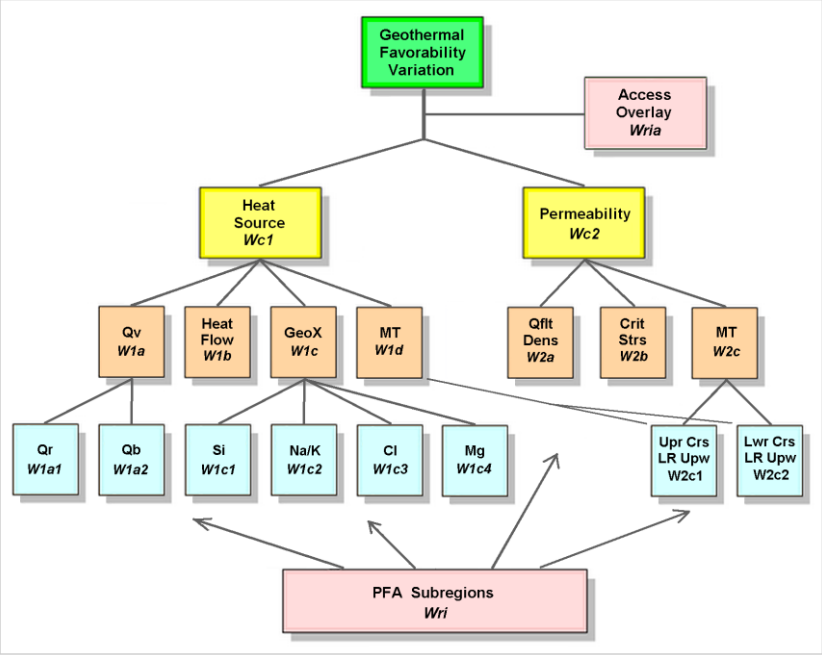

Figure 11: Idealized flow chart in a Multi-Criteria Decision Making (MCDM) framework illustrating factors or criteria considered for prioritizing subregions of the Eastern Great Basin PFA area. If all criteria data were sufficient to be represented in a fully rasterized form, higher level criteria weights such as for heat or permeability result from multiply-sum operations on sub rows. Weights Wijk may be derived from e.g. analytic hierarchy processing (AHP) or directly user specified. Diagram influenced by several publications (e.g., Saaty, 1977, 2008; Teknomo, 2006; Nouri et al., 2013; Boschmann et al., 2014; Wiki, 2015).

4.1 Heat Flow

The heat flow data are presented in Figure 12a according to probability that flux exceeds 80 mWm^{-2}. In contrast to a simple contour map where two widely spaced points of similar value can lead to an extrapolation of that value across large open spaces, kriged probability represents the uncertainty in defining a threshold where data are sparse or of poor quality. Thus the probability of exceeding the threshold is diminished in areas of poor data coverage.

As expected, our confidence that heat flow exceeds 80 is highest near known data which is clustered at geothermal systems such as Cove Fort, Roosevelt and Thermo. However, two other features stand out. First, probability of high heat flow extends substantially west of the Cove Fort producing system, essentially to the northern tip of the Mineral Mountains. This means that high heat flow corresponds with the Cinder Knolls (CK) MT conductor discussed with Figures 5 and 8. A second feature of note is that the high heat flow of the Thermo system appears to extend a considerable distance to the east from the producing area. This underscores the good fortune of bringing to light the extensive collection of industry TG hole results for this project.

4.2 Magnetotelluric Conductivity

Magnetotellurics has the advantage of intrinsic depth resolution due to the propagative wave nature of EM source fields. It also is sensitive to the presence of melts and fluids in large-scale fracture zones. We synthesize the MT results of Figure 5 by simply inverting to conductivity, which is more linearly related to abundance of fluid or melt, and computing an average over the 4.8 – 6.2 km depth

range. This emphasizes the conductive pipe-like features extending from the deep crustal transverse zone conductors toward the upper crust.

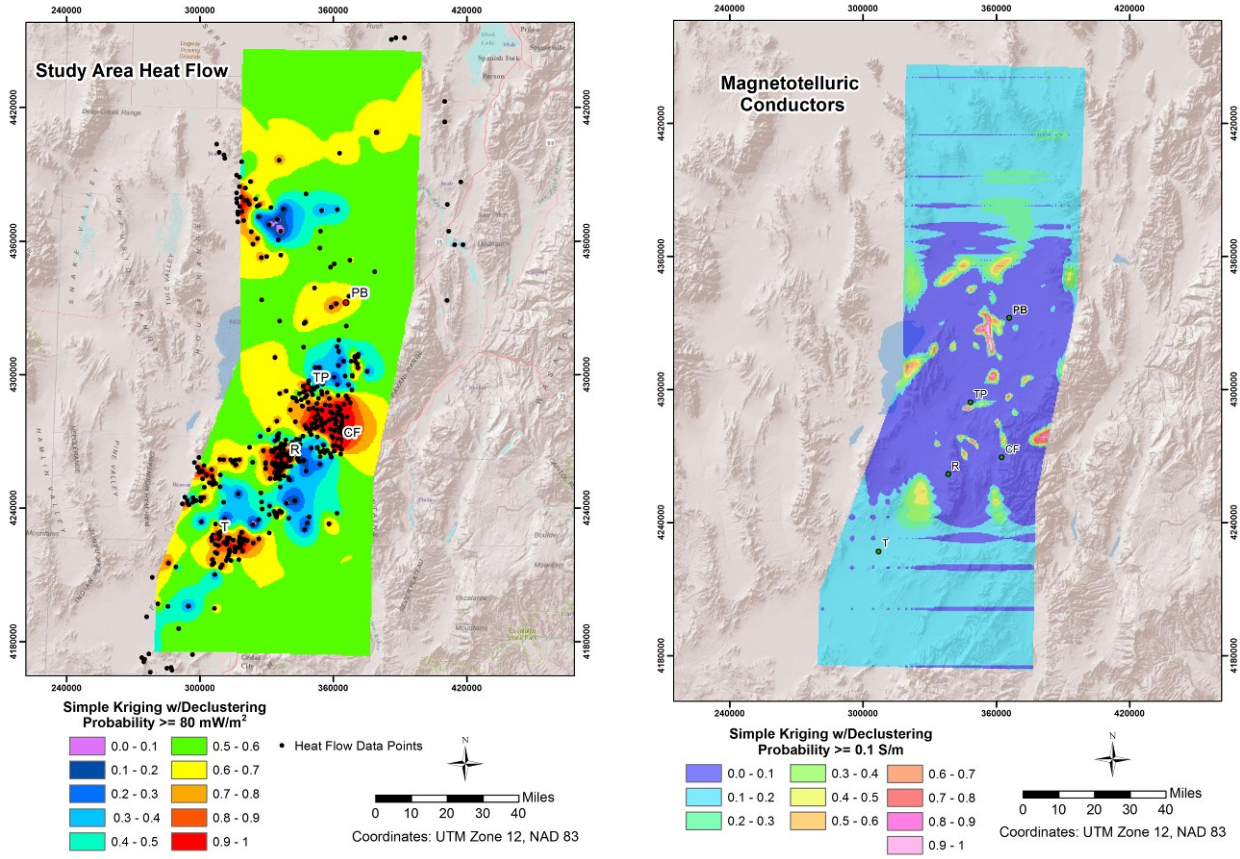

Figure 12: Left (a): Kriging map of probability (0 – 1) that heat flow exceeds 80 mWm-2 in the eastern Great Basin PFA area. Note that we use red as the color of highest probability (most favorability) and green as the color least favorable. Right (b): Kriging map of probability (0 – 1) that electrical conductivity exceeds 0.1 S/m in the central portion of the eastern Great Basin PFA area. Coarse mesh gridding artifacts are apparent as minor cosmetic streaking towards north and south model extremes outside area of MT data coverage.

The conductivity structure is transformed to a normalized range also by probability kriging and trimmed to the PFA area (Figure 12b). It closely ressembles straight conductivity but now is more appropriate for weighting in an MCDM process. Because these anomalies represent concentrations of melts or high temperature fluids that have upwelled to higher levels in the crust, MT conductivity can be a component both of the heat source and the permeability favorability criteria. The pipelike conductors of substantial vertical extent (rootedness to the deep crust) associated with Pavant Butte, Twin Peaks, Cinder Knoll and Cove Fort are apparent here.

4.3 Quaternary Volcanic Intrusives

The third component contributing to estimated heat source potential is presence of Quaternary volcanic intrusives. Units from the UGS data base were divided into basalt and rhyolite compositions (not plotted here; see e.g. Hintze and Kowallis, 2009). The more silicic ones are considered more favorable as they signify longer term accumulation and hybridization of magmas at mid-crustal levels (e.g., Blackett, 2007). In terms of kriged probability, outcrop is simply assigned unity weight, and lack of outcrop is zero. Original outcrop location was buffered outward by 2 km as a volume of heat influence according to studies of Norton (1991). Obvious silicic outcropping is associated with Twin Peaks and Roosevelt Hot Springs. Numerous basalt flows appear associated with the high-temperature Quaternary trend running the length of the state (Bendersky et al., 2012). Although we would prefer to key in on Q intrusives rather than flows, these are not distinguished on the state data base.

4.4 Fault Permeability

The primary quantities available for permeability estimation are fault density and the distribution of critically stressed zones. Simple fault density has been computed in the ArcGIS platform, transformed to kriged probability in the 0 – 1 range, and depicted in Figure 13a. The most apparent zones of dense faulting lie along the high gravity gradients (graben boundaries) of the Sevier Basin in the northern part of the PFA area, and off the east side of the Mineral Range including the Cove Fort area. However, numerous faults undoubtedly are hidden below recent alluvium of the major valleys such as Milford Valley, and the Escalante Desert further south. Critically stressed zones identified by procedures previously listed are shown in Figure 13b and tend to cluster near tips of fault

distributions. Here we have chosen to add the crustal scale Cove Fort and Blue Ribbon lineaments due to their apparent role in creating deep crustal dilatency and controlling the positions of localized low resistivity upwellings. In addition to those two lineaments discussed by Rowley et al (1998a,b, 2001), we have added the Twin Peaks-Meadow Hatton lineament identified from MT in Figure 5, and the E-W trending graben lineament extending from the Roosevelt Hot Springs producing system (Nielson et al., 1986).

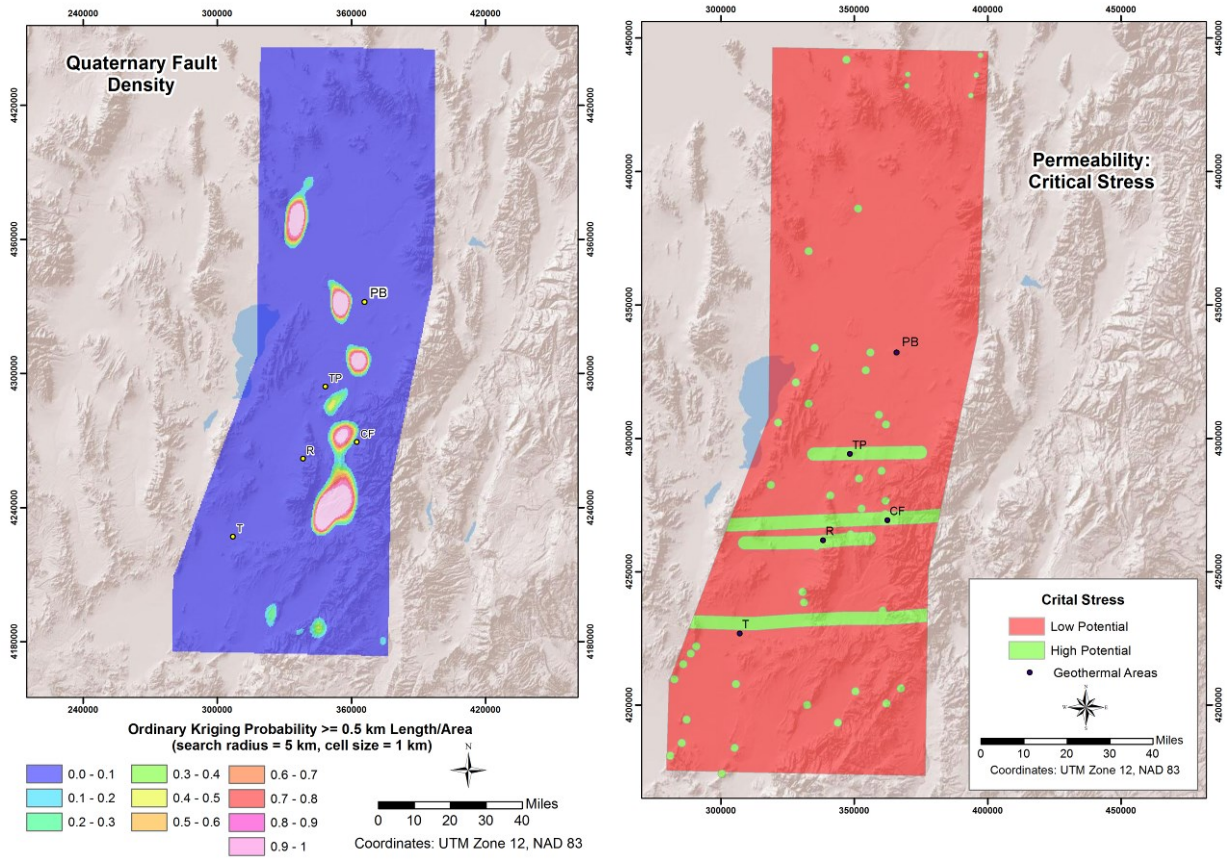

Figure 13: Left (a), Kriging map of probability (0 – 1) that fault density exceeds 0.5 km-1 for eastern Great Basin PFA area. Right (b), critically stressed zones in the PFA area including major E-W structural lineaments (see Figure 5).

4.5 Aqueous Geochemistry

Rock compositions fo a geothermal reservoir, its fluid sources, ages, and pathways, and deep reservoir temperatures are assessed using major element and isotopic fluid chemistry. Kriged threshold probabilities of T > 200^{o}C for the Na/K and Si > 100^{o}C geothermometers are shown in Figures 14a and b. Note the large, apparently coherent band of high probabilities according to Na/K in the southeast portion of the PFA area. Conventional wisdom holds that Na/K geothermometry is relatively robust to later fluid cooling or dilution (Nicholson, 1993). As noted by Simmons et al. (2015), that the Na/K implied temperatures are consistently higher than others like Si or even many of the directly measured reservoir fluid temperatures suggests that portions of many spring or well fluids have seen deeper and hotter conditions. Na/K probable temperatures of fluids in the Sevier Basin in the northern PFA area tend to be lower. In part this may reflect sparse sampling, or also contamination by upper crustal saline sediments.

The SiO2 geothermometry kriged probability, on the other hand, shows much less coherence (Figure 14b). Geothermal system and spring characteristics are much more individual, possibility due to variable flow paths, permeabilities, and fluid cooling on the way to the sampling. This highlights the fact that geothermal systems are discrete, 3-D entities often thwarting our ability to construct reliable statistical surfaces that can be used for reliable extrapolations and risk quantification. That should only be expected given understanding that systems form at zones of favorable structural dilatency and is in keeping with the discrete MT anomalies associated with geothermal systems.

Generally lower Mg values along a swath down the center of the PFA area suggests fluids have seen higher T at depth (Nicholson, 1993) (not plotted). This is roughly coincident with the trend of Quaternary basalt magmatism. However, there is much scatter and values exceeding 10 may reflect dominance by near surface waters or contamination by sedimentary rocks nearer surface. High values of Cl are expected and seen at Roosevelt Hot Springs given its very high temperatures and igneous crystalline basement. Somewhat elevated values are seen as well along a swath down the center of the PFA area, but again their scatter may reflect influence by near surface waters or contamination by sedimentary rocks nearer surface.

The highest helium isotope ratios are found at Roosevelt (2.25 R/Ra), Thermo (0.9 R/Ra), and Cove Fort (0.6 R/Ra), all showing evidence of mantle helium, with Roosevelt having the largest component. Mantle helium is interpreted to transport from intrusions of magma toward the surface in crustal scale fault zones, where it can then connect to convective geothermal fluid flow (e.g., Kennedy and van Soest, 2007; Wannamaker et al., 2007, 2011). Reported by Simmons et al. (2015), a well north of Cove Fort exhibited R/Ra of 1.66, a water well south of the Milford Valley Acord-1 well showed a value of 2.07, and a water well on east flank of Cricket Mtns bounding the Sevier Basin on its west side yielded R/Ra = 0.6. Mantle-derived magmatic contributions to upper crustal fluids appears increasingly common-place in this PFA area, with an implication of high-temperature crustal input.

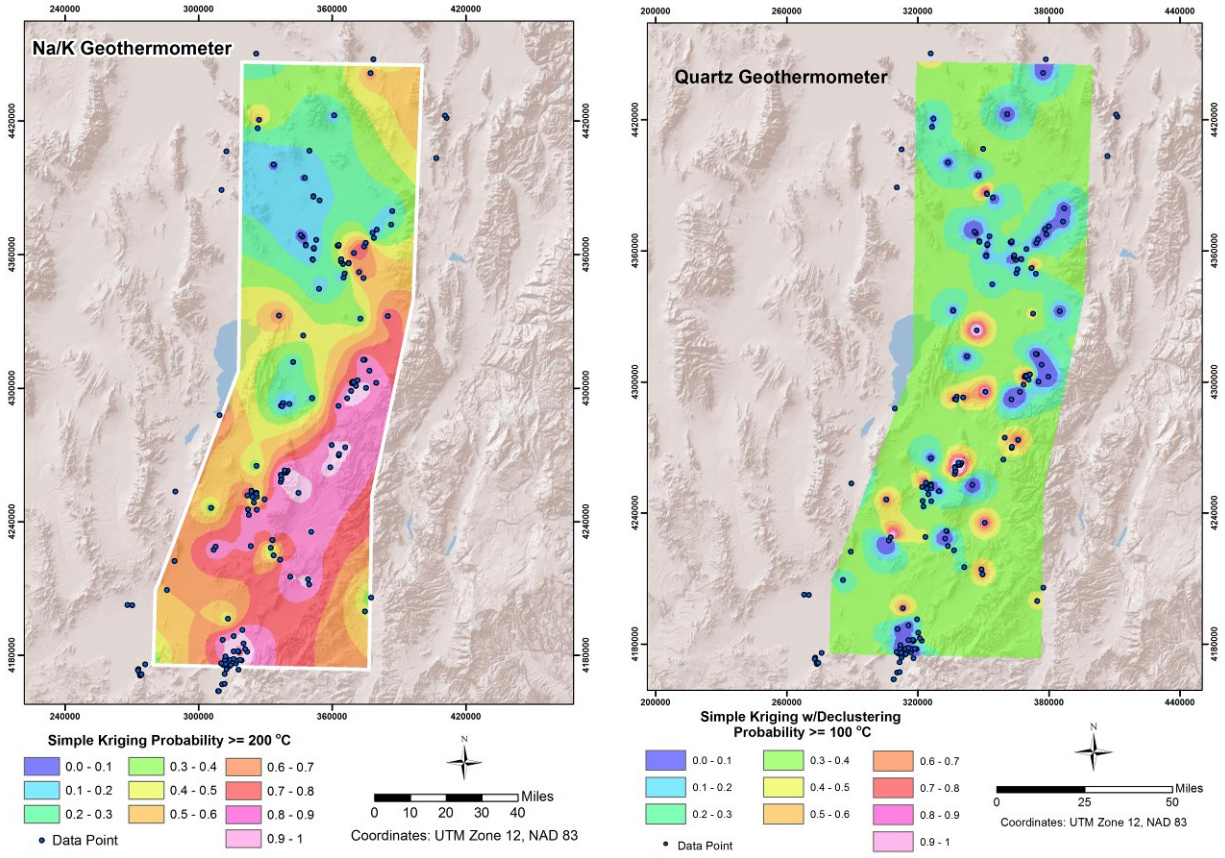

Figure 14: Kriged probabilities that temperatures according to fluid Na/K exceed 200°C (left, a), and according to Si exceed 100°C (right, b), for springs and well fluids in the eastern Great Basin PFA area.

4.6 Heat and Permeability Favorability Maps

In reference to the MCDM flow chart of Figure 11, heat source potential of the eastern Great Basin PFA area ideally could be estimated on the basis of Quaternary volcanism, heat flow, fluid geochemistry, and MT geophysics. Prior discussion distinguishes the ideal from reality in terms of which quantities can be combined straightforwardly in such a weighted sum procedure. Rhyolites are limited in spatial extent but their implications for stored crustal heat lead us to assign W1a1 = 0.8 and W1b1 = 0.2 for a sum of unity. Heat flow kriged probability is strongly influence by the locations of data, namely clustering around known producing geothermal systems such as Roosevelt. However, the fortuitously large amount of TG hole data that have become available to this project gives us confidence in some extrapolation away from current producers. Of the fluid geochemical indicators, only Na/K appears sufficiently spatially coherent to use as a kriged probability layer. Subsequently, total heat source potential is derived using the following weightings for Qv, heat flow, Na/K geochemistry, and MT conductivity: W1a = 0.2, W1b = 0.2, W1c = 0.2, and W1d = 0.4. However, because MT coverage only exists across part of the PFA area, we have also created a heat layer map with including MT as the remaining data sets do nominally span the PFA area. In this case, we choose W1a = 0.3, W1b = 0.4, W1c = 0.3.

The resulting heat potential CRS maps are displayed in Figure 15. Including MT structures in the heat CRS has significant influence on priority area and one sees high potential located near Cove Fort, Pavant Butte, Meadow Hatton and Twin Peaks where distinct MT conductors are positions. High priority occurs in the Cinder Knolls area and east of Cove Fort toward the Marysvale-Monroe areas east of our PFA domain. Nevertheless, given the clear association of steep crustal conductors with producing systems here and elsewhere in the Great Basin (Figure 2), this pin-pointing of priorities is considered valid. A high priority occurs near Roosevelt Hot Springs independent of MT due in part to its rhyolite dome outcrops. Without the MT structures (Figure 15b), priority areas generally are much broader and of lower contrast, although still quite useful and reveal the influence of other heat factors. For example, the broad domain of high Na/K-inferred temperatures becomes more apparent down the central southeastern portion of the PFA area. The westward extension of the large Cove Fort heat flow anomaly appears more prominently also.

For permeability potential, we rely predominantly on fault density and critical stressed zones, with secondary input from MT conductivity. We have weighted these W2a = 0.4, W2b = 0.4 and W2c = 0.2, with MT included under the assumption that conductive upwellings require some permeability for emplacement. Also, we deem it is appropriate to include the four major E-W structural lineaments either known before this project, or revealed through current data interpretation (Twin Peaks-Meadow Hatton MT lineament of Figure 14), in the critically stressed zone category. The resulting permeability potential map appears in Figure 16. One sees that permeability potential is dominated by the fault density and critically stressed zone locations as expected from the weighting.

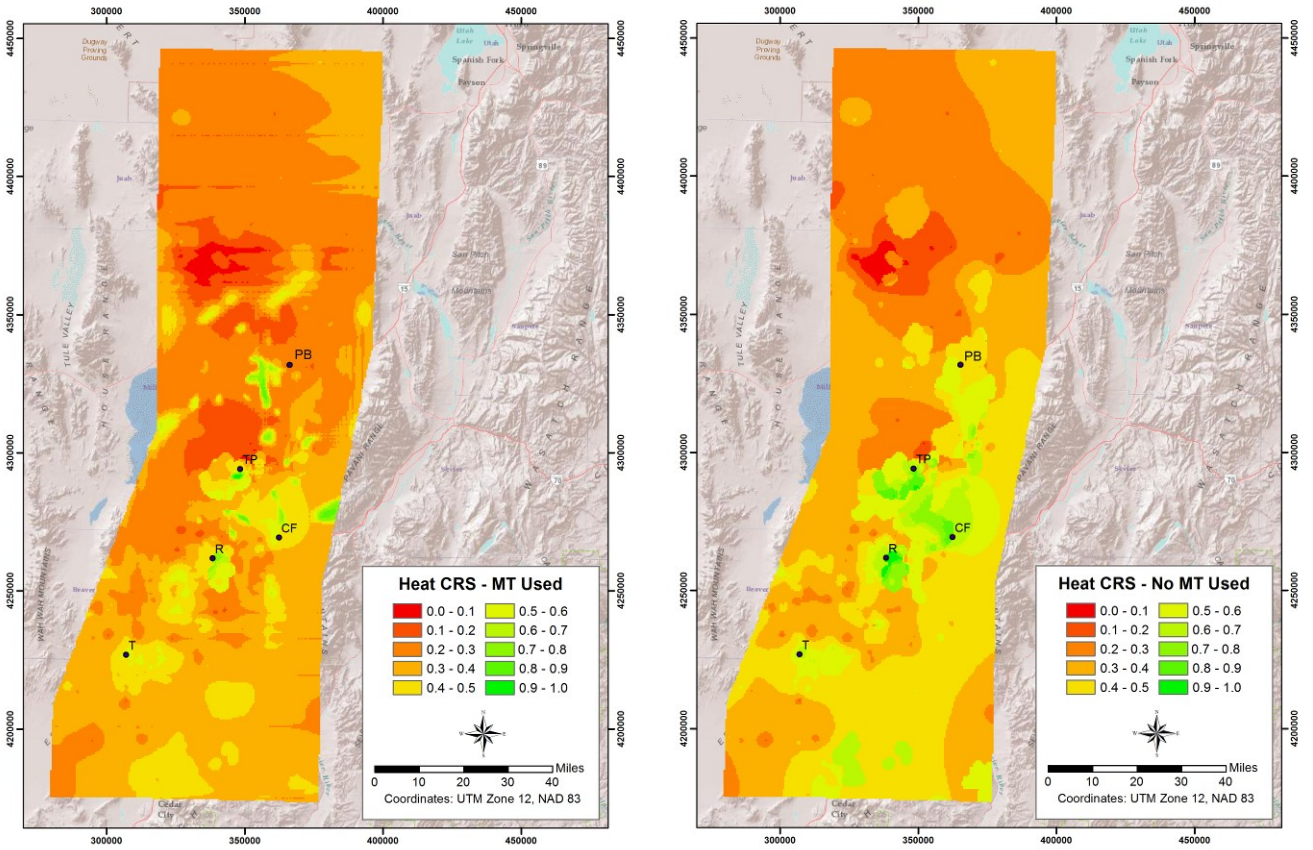

Figure 15: Two versions of heat potential CRS for the eastern Great Basin PFA area. Left (a), heat CRS which includes MT structures of the central portion of the study area. Right (b), heat CRS which excludes MT structures. Weighted sum results are normalized to a full range of unity for display in each map.

4.7 Access and Infrastructure

Access and infrastructure presents only limited challenges in this PFA area. Land ownership in the PFA area is shown in Figure 17. The eastern Great Basin region is dominated by Bureau of Land Management (BLM) and Utah State Institutional Trust Lands Authority holdings with a much lesser degree of USDA Forest Service. There are local significant portions of private holdings, particularly Murphy-Brown Inc in Milford Valley, but this is the same corporation which is being highly cooperative in the newly started Milford FORGE project supported by DOE (J. Moore, PI). Transmission lines appear to be sufficiently common and closeby should an economical geothermal resource be identified. These already serve Roosevelt Hot Springs, Cove Fort and Thermo, and also substantial recent wind and solar farm development in Milford Valley. Moreover, a 2 GWe DC power line runs from the Delta coal fired power plant just north of the town of Delta southward along the west side of Sevier Basin and Milford Valley to southern California, which does not appear in the transmission data base.

4.8 Final Resource and Favorability Mapping

The remaining task of this section is to compute final geothermal favorability by combining heat and permeability potential in a weighted sum, and by taking access and infrastructure into consideration. In this, we assign Wc1 = 0.65 and Wc2 = 0.35 in an effort to make sure heat sources are strongly represented, and to allow for a possibility that EGS resources could be identified even though natural permeability is absent. Final favorability maps are shown in Figure 18 both with and without MT contributing to the heat model.

This is an appropriate point to state that the weights assigned to different criteria in forming the CRS maps are person-defined for the rationales listed above. An alternative sometimes used for defining weights is the analytic hierarchy method (AHP) (Saaty, 1977, 2008;

Technomo, 2006; Boschmann et al., 2014). In this case, the subcriteria in a row, such as the four in the heat potential row of Figure 2 (Qv, HF, Na/K, MT), are pairwise compared for relative favorability. The favorability entries are then written into a small matrix (4x4 in the general case here) and the principal eigenvector of that matrix solved. In the case of a 2x2 matrix, the eigenvalue entries equal the original weight entries. The entries in an AHP matrix for an assessment such as this one are as user-defined as the ones we implement here. Our weights are not wide-ranging and experiments with changing relative values yields qualitative changes only in the map views.

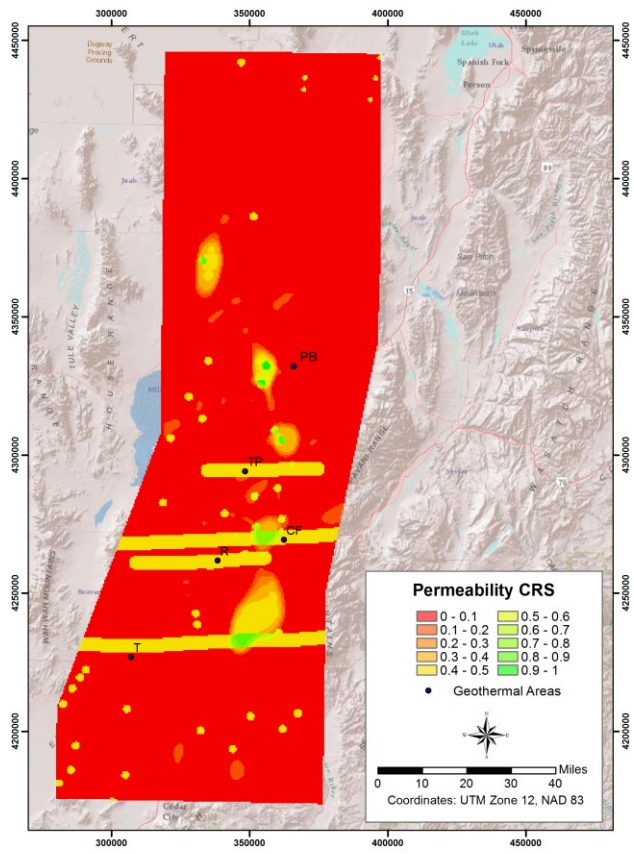

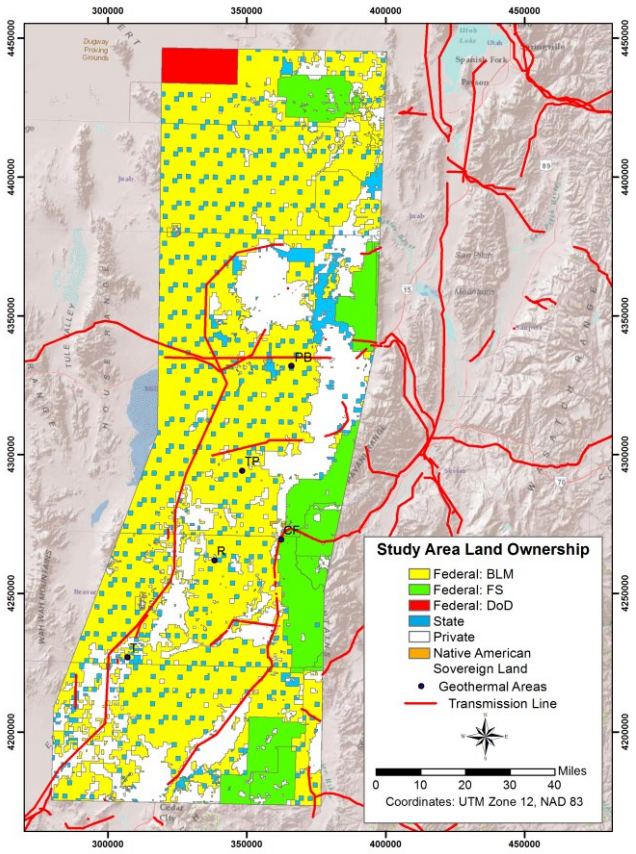

Figure 16 (left): Permeability potential CRS map of the eastern Great Basin PFA region. Figure 17 (right): Land ownership map and transmission lines for the eastern Great Basin PFA area.

CONCLUSIONS AND RECOMMENDATIONS

The overall favorability map and our knowledge of the region makes us very enthusiastic to pursue follow-up exploration (Figure 18). We believe the eastern Great Basin area could be promising for resources especially given heat potential and favorable structures. Given the likely control upon resource occurrence by the intersection of N-S and E-W faulting trends, a high priority area to assess would be an extension southward from the northern Mineral Mtns, past the E-W trending Roosevelt Hot Springs graben, and ultimately across the Blue Ribbon lineament. Furthermore, there is subtle evidence in the MT model for the broader Sevier Basin (refer to Figure 5) that ESE-WSW lineaments may be influencing conductive, presumably hot upwellings within the Sevier Basin proper such as Pavant Butte. Thus it could pay to widen the study area there modestly. Finally, at least two of the currently revealed localized structures, namely Cinder Knolls and Twin Peaks area, should receive denser investigation to achieve resolution sufficient for thermal gradient drilling.

Appropriate methods for followup include additional MT coverage including tightened spacing over 2-3 recognized reconnaissance anomalies to provide drilling targets, and swath coverage southward to seek other favorable locales on-trend with Roosevelt Hot Springs and within the region of high Na/K geothermometry. A deep thermal and structural nature to the MT low-resistivity anomalies should be verified by dedicated passive seismic arrays over two areas to resolve any correspondence with seismic swarms. New waveform subspace techniques are expected to lower the event threshold significantly, and double difference relocation methods will help pinpoint positions (Waldhauser and Ellsworth, 2000). Passive ^{3}He detectors (Dame et al., 2015) should be used to further confirm the deep thermal cause of targets for TG drilling. Detailed structural maps of 2-3 promising prospects will be created using high-res imagery (e.g., recent Google), multispectral Aster and panchromatic data, gravity infill, and relative fault age determinations.

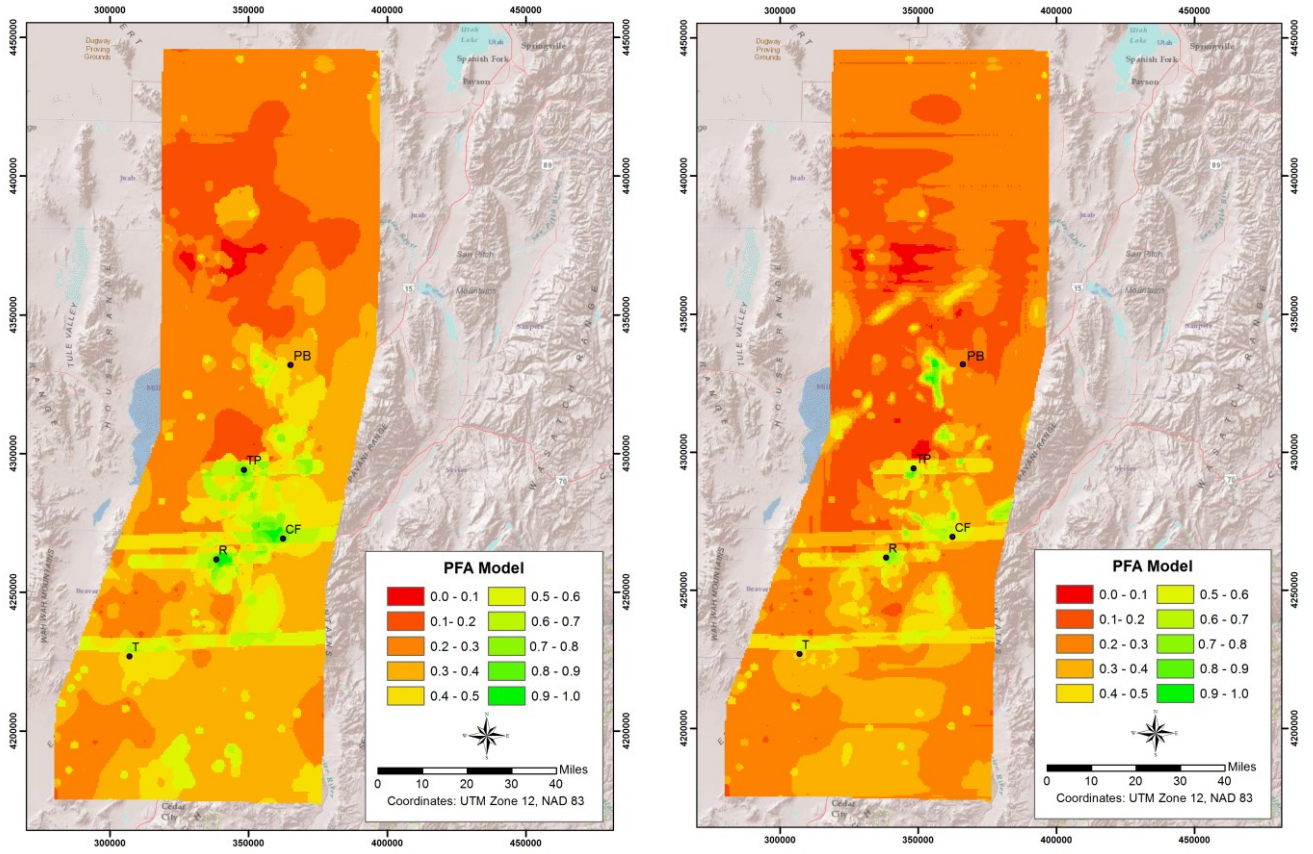

Figure 18a (left): Play fairway favorability map of the eastern Great Basin PFA region without MT included in the heat potential. Figure 18b (right): Play fairway favorability map of the eastern Great Basin PFA region with MT included in the heat potential.

ACKNOWLEDGEMENTS

This research was supported by U.S Dept of Energy contract DE-EE0006732. We are grateful to Dr. Michal Kordy for development and advice on application of the 3D MT inversion algorithm HexMT. Most of the MT soundings were acquired by Quantec Geoscience Inc.

REFERENCES

Allis, R. G., M. Gwynn, C. Hardwick, S. Kirby, J. Moore, and D. Chapman, Re-evaluation of the pre-development thermal regime of Roosevelt Hot Springs geothermal system, Utah: Proc. 40th Workshop on Geothermal Reservoir Engineering, Stanford University, Stanford, CA, **204**, 12 pp., 2015a.

Allis, R. G., C. Hardwick, M. Gwynn, and S. Johnson, Pavant Butte geothermal prospect revisited: Geothermal Resources Council Transactions, **39**, 2015b.

Arabasz, W. J., R. Burlacu, and K. L. Pankow, An overview of historical and contemporary seismicity in central Utah, in Willis, C. G., M. D. Hylland, D. L. Clark, and T. C. Chidsey, Jr., eds., Central Utah - Diverse Geology of a Dynamic Landscape, Utah Geological Association Publication, **36**, 237–253, 2007.

Bendersky, C., T. Plank, D. W. Forsyth, E. H. Hauri, C-T. Lee, and D. Forsyth, Magmatism and lithospheric destruction along the Colorado Plateau margin: EOS, Transactions AGU, Fall Meeting, San Francisco, California, 2012.

Blackett, R. E., Review of selected geothermal areas in southwestern Utah: Geothermal Resources Council Transactions, **31**, 111-116, 2007.

Blackett, R. E., and S. I. Wakefield, Geothermal resources of Utah, a digital atlas of Utah's geothermal resources: Utah Geological Survey, **OFR-397**, CD-ROM, 2002.

Boschmann, D. E., J. L. Czajkowski, and J. D. Bowman, Geothermal favorability model of Washington State, Washington State Dept. of Natural Resources, **OFR 2014-2**, 20 pp., 2014.

Capuano, R. M., and D. R. Cole, Fluid-mineral equilibria in a hydrothermal system: Geochimica Cosmochimica Acta, **46**, 1353-1364, 1982.

Cole, D. R., Chemical and Isotopic investigation of warm springs associated with normal faults in Utah: Journal of Volcanology and Geothermal Research, **16**, 65-98, 1983.

Dame, B. E., D. K. Solomon, W. C. Evans, and S. E. Ingebritsen, Developing a new, passive diffusion sampler suite to detect helium anomalies associated with volcanic unrest: Bulletin of Volcanology, **77**, 17 pp, 2015.

Edwards, M. C.., and D. S. Chapman, A geothermal assessment of the Basin and Range province in western Utah: Report to Utah Geological Survey, UGS award 120000, 114 pp., 2013.

Faulds, J. E., N. H. Hinz, G. M. Dering, and D. L. Siler, The hybrid model – the most accommodating structural setting for geothermal power generation in the Great Basin, western USA: Geothermal Resources Council Transactions, **37**, 3-10, 2013.

Fraser, A. J., A regional overview of the exploration potential of the Middle East: a case study in the application of play fairway risk mapping techniques: in Vining, B. A., and S. C. Pickering, eds., Petroleum geology: from mature basins to new frontiers, Proc. 7th Petroleum Geology Conference, Geological Society of London, 791-800, 2010.

Fournier, R. O., Water geothermometers applied to geothermal energy: in Applications of Geochemistry in Geothermal Reservoir Development, UNITAR-UNDP, F. D'Amore, ed., 37-69, 1991.

Giggenbach, W. F., The origin and evolution of fluids, in Magmatic-hydrothermal systems: Geochemistry of Hydrothermal Ore Deposits, 3rd edition, John Wiley & Sons, 737-796, 1997.

Hardwick, C. L., R. Allis, and P. E. Wannamaker, Observations and implications of magnetotelluric data for resolving stratigraphic reservoirs beneath the Black Rock desert, Utah, USA: Geothermal Resources Council Transactions, **39**, 2015.

Harris, D., Subspace detectors: Theory: Lawrence Livermore National Laboratory Report, **UCRL-TR-222758**, Lawrence Livermore National Laboratory, Livermore, California, 48 pp, 2006.

Harris, D., and T. Paik, Subspace detectors: Efficient implementation: Lawrence Livermore Natl. Lab. Rep., UCRL-TR-223177, Lawrence Livermore National Laboratory, Livermore, California, 36 pp, 2006.

Henley, R. W., and A. J. Ellis, Geothermal systems ancient and modern: A geochemical review: Earth-Science Reviews, 19, 1-50, 1983.

Hintze, L. F, and B. Kowallis, Geologic History of Utah, Brigham Young University Press, 202 pp, 2009.

Kennedy, B. M., and van Soest, M. C., 2007, Flow of mantle fluids through the ductile lower crust: helium isotope trends: Science, **318**, p. 1433-1436.

King, D., and E. Metcalfe, Rift zones as a case for advancing geothermal occurrence models: Proc. 38th Workshop on Geothermal Reservoir Engineering, Stanford, CA, SGP-TR-198, 1578-1588, 2013.

Kordy, M. A., P. E. Wannamaker, V. Maris, E. Cherkaev, and G. J. Hill, 3-D magnetotelluric inversion using deformed hexahedral edge finite elements and direct solvers parallelized on SMP computers, Part I: forward problem and parameter jacobians: Geophysical Journal International, **204**, 74-93, 2016a.

Kordy, M. A., P. E. Wannamaker, V. Maris, E. Cherkaev, and G. J. Hill, 3-D magnetotelluric inversion using deformed hexahedral edge finite elements and direct solvers parallelized on SMP computers, Part II: direct data-space inverse solution: Geophysical Journal International, **204**, 94-110, 2016b.

Kreemer, C. W. C. Hammond, G. Blewitt, A. A. Holland and R. A. Bennett, A geodetic strain rate model for the Pacific-North American plate boundary, western United States: Nevada Bureau of Mines and Geology, Map 178, scale 1:1,500,000, 2012.

Nelson, S. T., and D. G. Tingey, Time-transgressive and extension-related basaltic volcanism in southwest Utah and vicinity: Geological Society of America Bulletin, **109**, 1249-1265, 1997.

Nielson, S. H. Evans and B. S. Sibbett, Magmatic, structural and hydrothermal evolution of the Mineral Mountains intrusive complex, Utah: Geological Society of America Bulletin, **97**, 765-777, 1986.

Nicholson, K., Geothermal Fluids: Chemistry and Exploration Techniques: Springer, Berlin, 263 pp., 1993.

Norton, D. L., Fluid and heat transport phenomena typical of copper-bearing pluton environments: in, Advances in Geology of the Porphyry Copper Deposits, S. R. Titley ed., The University of Arizona Press, 59-72, 1983.

Nouri, R., P. Afzal, M. Arian, M. Jafari, and F. Feizi, Reconnaissance of copper and gold mineralization using analytical hierarchy process (AHP) in the Rudbar 1:100,000 map sheet, northwest Iran: Journal of Mining and Metallurgy, **49 A (1)**, 9-19, 2013.

Reasenberg, P., Second-order moment of central California seismicity: 1969-82: Journal of Geophysical Research, **90**, 5479– 5495, 1985.

Rowley, P. D., Cenozoic transverse zones and igneous belts in the Great Basin, western United States: their tectonic and economic implications: in Faulds, J. E., and J. H. Sterart, eds., Accommodation zones and transfer zones: the regional segmentation of the Basin and Range province, Geological Society of America, Special Paper **323**, 195-228, 1998.

Rowley, P. D., C. G. Cunningham, T. A. Steven, H. H. Mehnert, and C. W. Naeser, Cenozoic Igneous and Tectonic Setting of the Marysvale Volcanic Field and Its Relation to Other Igneous Centers in Utah and Nevada: in, Friedman, J. D., and Huffman, A.C., Jr., ed., Laccolith Complexes of Southeastern Utah: Tectonic Control and Time of Emplacement -Workshop Proceedings: U.S. Geological Survey Bulletin **2158**, 167-201, 1998.

Rowley, P. D., and G. L. Dixon, The Cenozoic evolution of the Great Basin area, U.S.A. - new interpretations based on regional geologic modeling: in, The Geological Transition: Colorado Plateau to Basin and Range, Proc. J. Hoover Mackin Symposium, ed. by M. C. Erskine, J. E. Faulds, J. M. Bartley and P. Rowley, UGA/AAPG Guidebook **30/GB78**, Cedar City, Utah, September 20-23, 1-38, 2001.

Saaty, T. L., A scaling method for priorities in hierarchical structures: Journal of Mathematical Psychology, **15**, 234-281, 1977.

Saaty, T. L., Decision making wiwth the analytic hierarchy process: International Journal of Services Sciences, **1(1)**, 83-98, 2008.

Schmandt, B., and F.-C Lin, P and S wave tomography of the mantle beneath the United States: Geophysical Research Letters, **41**, 6342-6349, 2014.

Simmons, S., S. Kirby, J. Moore, P. Wannamaker, and R. Allis, Comparative analysis of fluid chemistry from Cove Fort, Roosevelt and Thermo: implications for geothermal resources and hydrothermal systems on the east edge of the Great Basin: Geothermal Resources Council Transactions, **39**, 2015.

Siler, D. L., B. M. Kennedy, P. E. Wannamaker, Regional lithospheric discontinuities as guides for geothermal exploration: Geothermal Resources Council Transactions, **38**, 39-47, 2014.

Teknomo, K., Analytic hierarchy process (AHP) tutorial: on-line web tutorial, http://people.revoledu.com/kardi/tutorial/AHP/, 2006.

Waldhauser F. and W. L. Ellsworth, A double-difference earthquake location algorithm: Method and application to the northern Hayward fault, Bulletin of the Seismological Society of America, 90, 1353-1368, 2000.

Wannamaker, P. E., W. M. Doerner, and D. P. Hasterok, Integrated dense array and transect MT surveying at Dixie Valley geothermal area, Nevada; structural controls, hydrothermal alteration and deep fluid sources, Proc. 32nd Workshop on Geothermal Reservoir Engineering, Stanford, CA, **SGP-TR-183**, 6 pp, 2007.

Wannamaker, P. E., D. P. Hasterok, J. M. Johnston, J. A. Stodt, D. B. Hall, T. L. Sodergren, L. Pellerin, V. Maris, W. M. Doerner, and M. J. Unsworth, Lithospheric dismemberment and magmatic processes of the Great Basin-Colorado Plateau transition, Utah, implied from magnetotellurics: Geochemistry, Geophysics, Geosystems, **9**, Q05019, doi:10.1029/ 2007GC001886, 36 pp, 2008.

Wannamaker, P. E., V. Maris, D. Hasterok, and W. Doerner, Crustal Scale Resistivity Structure, Magmatic-Hydrothermal Connections, and Thermal Regionalization of the Great Basin: Geothermal Resources Council Transactions, **35**, 1787-1790, 2011.

Wannamaker, P. E., V. Maris, J. Sainsbury, and J. Iovenitti, Intersecting fault trends and crustal-scale fluid pathways below the Dixie Valley geothermal area, Nevada, inferred from 3D magnetotelluric surveying, Proc. 38th Workshop on Geothermal Reservoir Engineering, Stanford, CA, **SGP-TR-198**, 9 pp, 2013a.

Wannamaker, P. E., J. Faulds and B. M. Kennedy, Integrating magnetotellurics, soil gas geochemistry and structural analysis to identify hidden, high enthalpy, extensional geothermal systems, Annual Report to the U.S. DOE/GTP, Contract DE-EE0005514, 13 pp., 2013b.

Wannamaker, P. E., V. Maris, and C. Hardwick, Basin and rift structure of the central Black Rock Desert, Utah, and initial thermal implications, from 3D magnetotellurics: Geothermal Resources Council Transactions, **37**, 41-44, 2013c.

Wannamaker, P. E., G. D. Nash, J. N. Moore, K. L. Pankow, Structurally controlled geothermal systems, eastern Great Basin extensional regime, Utah: Geothermal Resources Council Transactions, **38**, 2014.

Wisian, K. W., and D. D. Blackwell, Numerical modeling of Basin and Range geothermal systems: Geothermics, **33**, 713-741, 2004.